Open Chem., 2016; 14: 363–376

Research Article **Open Access**

Vladislav A. Sadykov, Mikhail N. Simonov, Natalia V. Mezentseva, Svetlana N. Pavlova, Yulia E. Fedorova, Aleksei S. Bobin, Yulia N. Bespalko, Arcady V. Ishchenko, Tamara A. Krieger, Tatiana S. Glazneva, Tatyana V. Larina, Svetlana V. Cherepanova, Vasilii V. Kaichev, Andrey A. Saraev, Yurii A. Chesalov, Aleksandr N. Shmakov, Anne-Cecile Roger, Andrzej Adamski

Ni-loaded nanocrystalline ceria-zirconia solid solutions prepared via modified Pechini route as stable to coking catalysts of CH_4 dry reforming

DOI 10.1515/chem-2016-0039
received November 5, 2016; accepted November 27, 2016.

Abstract: Mixed nanocrystalline Ce-Zr-O oxides (Ce/Zr = 1 or 7/3) were prepared by modified Pechini route using ethylene glycol solutions of metal salts. Detailed characterization of their real structure and surface properties by X-ray diffraction on synchrotron radiation with the full-profile Rietveld analysis, high resolution electron microscopy with elemental analysis, Raman spectroscopy, UV-Vis and X-ray photoelectron spectroscopy revealed a high homogeneity of cations distribution in nanodomains resulting in stabilization of disordered cubic phase. This provides a high dispersion of NiO loaded on these mixed oxides by wet impregnation, a high reactivity and mobility of oxygen in these catalysts and strong interaction of Ni with support in the reduced state. This helps to achieve a high activity and coking stability of developed catalysts in CH_4 dry reforming in feeds with CH_4 concentration up to 15% and CH_4/CO_2 ratio =1.

***Corresponding author: Vladislav A. Sadykov:** Boreskov Institute of catalysis, Novosibirsk, 630090, Russia; Novosibirsk State University, Novosibirsk, 630090, Russia, E-mail: sadykov@catalysis.ru
Mikhail N. Simonov, Natalia V. Mezentseva, Aleksei S. Bobin, Arcady V. Ishchenko, Tamara A. Krieger, Tatiana S. Glazneva, Tatyana V. Larina, Aleksandr N. Shmakov: Boreskov Institute of catalysis, Novosibirsk, 630090, Russia; Novosibirsk State University, Novosibirsk, 630090, Russia
Svetlana N. Pavlova, Yulia E. Fedorova, Yulia N. Bespalko, Svetlana V. Cherepanova, Vasilii V. Kaichev, Andrey A. Saraev, Yurii A. Chesalov: Boreskov Institute of catalysis, Novosibirsk, 630090, Russia
Anne-Cecile Roger: University of Strasbourg, Strasbourg, F-67087, France
Andrzej Adamski: Jagiellonian University, Krakow, Poland

Keywords: methane dry reforming, Ce-Zr-O oxide, Ni stabilization, coking stability

1 Introduction

Dry reforming of methane (DR) is now attracting a lot of attention because it converts cheap greenhouse gases into syngas with H_2/CO ratio ~ 1 the most suitable for synfuel production [1-4]. However, the commercial application of DR reaction is limited due to the lack of stable to coking industrial catalysts. Catalysts comprised of mixed ceria-zirconia oxides with supported precious metals, Co and/or Ni demonstrate promising activity and coking stability in this reaction, which is explained by a high lattice oxygen mobility of these oxides and strong metal –support interaction [3-10]. While Ni-loaded catalysts are clearly much more attractive for wide-scale practical application than those containing Pt-group metals, their performance strongly depends upon the nanoscale uniformity of the components distribution in Ce-Zr-O oxides affecting their oxygen mobility and reactivity [5-8]. Thus, for catalysts based on mixed oxides with a large inhomogeneity comprised of domains enriched by Ce or Zr, respectively, prepared via traditional solid-state sintering, precipitation or Pechini routes (water solutions were used in last two methods) and Ni being loaded by the wet impregnation, a rapid deactivation in DR due to coking was observed [5, 8, 11]. On the other hand, performance was quite stable for catalysts with enhanced homogeneity prepared via different versions of more expensive surfactant-assisted (cetyltrimethylammonium bromide) sol-gel/microemulsions routes [6]. A high homogeneity was also demonstrated for mixed Ce-Zr-O oxides prepared by sol-gel method using ethanol solutions of Ce and Zr salts with addition of acetylacetonate as complexing agent

[12]. Since in the inexpensive Pechini route such solvent as ethylene glycol without addition of water or ethanol still has not been used, it is certainly of interest to try such a modification of this route to check possibility of improving homogeneity of ceria-zirconia solid solutions, and, hence, providing a high coking stability of Ni-loaded catalysts in CH_4 DR.

This works presents results of such research for the case of mixed nanocrystalline Ce-Zr-O oxides (Ce/Zr = 1 or 7/3) loaded with Ni with detailed characterization of their real structure, surface properties and reactivity by unique combination of methods including X-ray diffraction on synchrotron radiation, TEM with EDX, X-ray photoelectron spectroscopy (XPS), UV-Vis, Raman, Fourier-transform Infrared Spectroscopy of adsorbed CO, temperature-programmed reduction by H_2 (H_2 TPR) along with estimation of their activity and coking stability in CH_4 dry reforming in feeds with CH_4 concentration up to 15% and CH_4/CO_2 ratio =1.

2 Experimental

2.1 Catalyst Preparation

Dispersed Ce-Zr-O mixed oxides were prepared by a modified polymerized polyester precursor (Pechini) route (following in general earlier described procedures [13] but using ethylene glycol instead of water) and calcined at 500 °C. At a constant stirring, metal nitrates were dissolved in ethylene glycol mixture with citric acid followed by ethylenediamine addition dropwise. The mole ratios of citric acid (CA), ethylene glycol (EG) (either ethanol) and ethylenediamine (ED) to the total metal ions in the solution were equal to 3.75:11.25:3.75:1. This viscous liquid was evaporated on a hot plate increasing the temperature to 100 °C for 5 h followed by heating at 150 °C for the next 5 h. A solid resin thus formed was burned under air at 500 °C. All reagents used for synthesis were of the ''chemical pure grade''. Ni (in amounts of 2-5 wt.% Ni) was loaded by incipient wetness impregnation with Ni nitrate solution followed by drying and calcination under air at 500 °C.

2.2 Catalyst Characterization

2.2.1 Specific surface area

The specific surface area of samples was determined from the Ar thermal desorption data by using BET method.

2.2.2. X-Ray Diffraction (XRD)

SXRD (Synchrotron X-ray Diffraction) experiments of crystal structure parameters were performed at "Precision Diffractometry" station in Siberian Synchrotron and Terahertz Radiation Center of the Budker Institute of Nuclear Physics (Siberian Branch, Russian Academy of Sciences) using synchrotron radiation with λ=1.546 Å for measurements in the 2θ range 10-70° with a step of 0.05° and position-sensitive parallax-free OD-3M detector [14]. The structural parameters such as lattice constants and site occupancies were refined using the full-profile Rietveld analysis (TOPAS software, Bruker, Germany). Average crystallites sizes and strains were also determined by means of TOPAS where widths and shapes of diffraction peaks are taken into account. Besides, quantitative phase analysis was made for the samples 5%Ni/$Ce_{0.5}Zr_{0.5}O_2$ and 5%Ni/$Ce_{0.7}Zr_{0.3}O_2$ by means of Rietveld analysis.

2.2.3 High Resolution Transmission Electron Microscopy (TEM) and Energy Dispersive X-Ray Spectroscopy (EDX)

Transmission Electron Microscopy (TEM) micrographs were obtained with a JEM-2010 instrument (lattice resolution 1.4 Å, acceleration voltage 200 kV). Analysis of the local elemental composition was carried out by using an energy-dispersive EDX spectrometer equipped with Si(Li) detector (energy resolution 130 eV). To prepare samples for TEM studies, powders were dispersed in ethanol and suspensions were subjected to ultrasonic treatment at 35 kHz. The suspension was poured onto a holey carbon substrate on a Mo grid and dried at 20 °C [13].

2.2.4 Raman and UV-Vis Diffuse Reflection (DR) Spectroscopy

The Raman scattering measurements were carried out using a 100/S-Bruker Raman Fourier Spectrometer (the 1064 nm line of an Nd-YAG laser was used for excitation). UV-Vis DR spectra were recorded on a Shimadzu UV-2501 PC (Japan) spectrophotometer with ISR-240A diffuse reflection attachment in relation to $BaSO_4$ in a wavelength range of 190-900 nm (11000-53000 cm^{-1}).

2.2.5 X-ray photoelectron spectroscopy (XPS)

X-ray photoelectron spectroscopy was applied for the chemical analysis of the Ni-loaded catalysts. XPS studies

were performed on an X-ray photoelectron spectrometer (SPECS Surface Nano Analysis GmbH, Germany) equipped with an X-ray source XR-50 with a twin Al/Mg anode, and a hemispherical electron energy analyzer PHOIBOS-150. The core-level spectra were obtained using the non-monochromatic AlK_α radiation (hν= 1486.6 eV) under ultrahigh vacuum conditions. Binding energies of the photoemission peaks were corrected to the C*1s* peak at 284.8 eV corresponding to carbon contamination. Relative element concentrations were determined from the integral intensities of XPS peaks using the cross-sections according to Scofield [15]. For detailed analysis the spectra were fitted into several peaks after the background subtraction by the Shirley method. The fitting procedure was performed using CasaXPS software. The line shapes were approximated by the multiplication of Gaussian and Lorentz functions.

2.2.6 FTIRS of adsorbed CO

The surface properties of $Ni/Ce_xZr_yO_2$ samples were studied by low-temperature Fourier-transform infrared spectroscopy (FTIRS) of adsorbed carbon monoxide. For registering IR spectra, the samples were pressed into pellets of 2-2.5 cm^2 area with a total weight of 20-40 mg. The pellet was placed into an IR cell and pretreated according to one of the following procedures:

1) in oxygen atmosphere: the sample was heated up to 673 K in an oxygen atmosphere (100 Torr of O_2) and calcined for 1 h, then it was cooled down to room temperature and evacuated to a residual pressure of at least 10^{-3} Torr;

2) in hydrogen atmosphere: the sample was heated up to 673 K in vacuum, then 100 Torr of H_2 were introduced into the cell, and the sample was calcined in hydrogen atmosphere for 1 h, then it was evacuated to a residual pressure of at least 10^{-3} Torr and cooled down to room temperature.

IR spectra of samples before and after CO adsorption were registered at 77 K using FTIR-8300 Shimadzu spectrometer in the range of 400-6000 cm^{-1} with a resolution of 4 cm^{-1} and a number of scans 100. CO pressure at adsorption varied from 0.1 to 10 Torr. After registering the spectra at the liquid nitrogen temperature (77K), a cell was heated to room temperature and the spectrum was registered again.

2.2.7 H_2 TPR

Reactivity of Ni-loaded samples was studied using temperature- programmed reduction (TPR) by H_2 (10% H_2 in Ar, feed rate 2.5L h^{-1}, temperature ramp from 25 to 900 °C at 10° min^{-1}). The experiments were carried out in kinetic installations equipped with GC Tcvet-500 [16].

2.2.8 Catalytic activity

The dry reforming reaction was carried out over the preoxidized or prereduced catalysts using quartz reactors and a flow installation equipped with GC and on-line IR absorbance, electrochemical and polarographic gas sensors for different components as described elsewhere [16]. The reaction was studied in the temperature-programmed mode (1%CH_4 +1%CO_2 in He, contact time 0.008 s) as well as in the steady-state conditions at temperatures up to 800–850 °C and contact time 0.008 s using feeds with CH_4 content up to 15% and CO_2 /CH_4 ratio = 1.

3 Results and Discussion

3.1 Structural characteristics

3.1.1 XRD

The X-ray diffraction (XRD) patterns for the $Ce_{0.5}Zr_{0.5}O_2$, 5%$Ni/Ce_{0.5}Zr_{0.5}O_2$ and 5%$Ni/Ce_{0.7}Zr_{0.3}O_2$ samples are shown in Figure 1. The XRD pattern of $Ce_{0.5}Zr_{0.5}O_2$ sample contains peaks of a fluorite-type structure [17]. The XRD pattern of 5%$Ni/Ce_{0.5}Zr_{0.5}O_2$ sample also contains peaks of the fluorite-type structure but these peaks are slightly shifted to smaller angles. The XRD pattern of 5%$Ni/Ce_{0.7}Zr_{0.3}O_2$ also contains peaks of a fluorite-type structure. These peaks have almost the same positions as peaks of $Ce_{0.5}Zr_{0.5}O_2$. Besides, additional small peaks of NiO are observed in the XRD patterns of 5%$Ni/Ce_{0.5}Zr_{0.5}O_2$ and 5%$Ni/Ce_{0.7}Zr_{0.3}O_2$ samples (arrows).

Full-profile Rietveld refinement for the $Ce_{0.5}Zr_{0.5}O_2$ sample is shown in the Figure 2. The XRD pattern was indexed in the cubic unit cell setting with Fm3m space group as well as in the setting of tetragonal unit cell with $P4_2/nmc$ space group. Both settings give close R-factors (~20%) and the same normalized unit cell volumes (Table 1): the cubic unit cell volume is almost twice larger than the tetragonal one. Similar results were earlier obtained by Abniyaz et al for $Ce_{0.5}Zr_{0.5}O_2$ sample prepared by the hydrothermal method [18], which was assigned to t''-form of the tetragonal phase with pronounced oxygen displacements. Note that for $Ce_{0.5}Zr_{0.5}O_2$ sample prepared

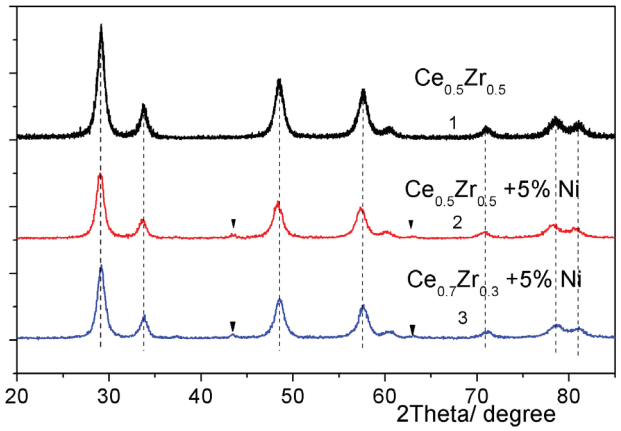

Figure 1: XRD patterns of $Ce_{0.5}Zr_{0.5}O_2$, 5%Ni/$Ce_{0.5}Zr_{0.5}O_2$ and 5%Ni/$Ce_{0.7}Zr_{0.3}O_2$ samples.

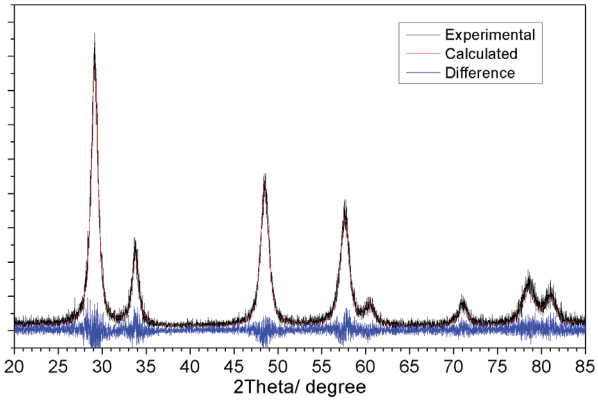

Figure 2: Full-profile Rietveld refinement for $Ce_{0.5}Zr_{0.5}O_2$ sample.

in this work (similar to those in [18]), diffraction peaks are symmetric (Fig.1), while for sample prepared with a traditional Pechini route using water solutions a strong asymmetry of peaks revealing coexisting domains enriched by Ce and Zr, respectively, was observed [14, 19]. Hence, apparently modification of the Pechini preparation route using ethylene glycol solutions allows to provide a homogeneity of cations distribution between domains [17, 20, 21].

The average crystallite size of $Ce_{0.5}Zr_{0.5}O_2$ is about 8-10 nm. Strains are large enough and equal to 0.27 that can be connected with the replacement of smaller zirconium cations by larger cations of cerium (rZr^{4+}=0.8 Å; rCe^{+} =1.01 Å) and disordering of nanodomains boundaries [23, 24]. Refined occupancy of oxygen sites is 0.96, which means either the presence of Ce^{3+} or the displacement of oxygen atoms in the fluorite structure from the 8c regular positions to interstices [18-22]. Enhanced value of the lattice parameter for $Ce_{0.5}Zr_{0.5}O_2$ (a=5.3236(3) Å) as compared with that for the sample prepared by traditional Pechini route with water solutions (5.285 Å) [19] suggests a higher content of Ce^{3+} cations due to apparently more reducing conditions of synthesis as well as a higher content of residual water and hydroxyls retained in the lattice of nanocrystalline sample calcined at moderate temperatures and stored under contact with air [18, 23, 24].

Full-profile Rietveld refinement for 5%Ni/$Ce_{0.5}Zr_{0.5}O_2$ sample is shown in Figure 3. Estimated by Rietveld analysis NiO content is about 6 weight %. It seems that a part of Ni is incorporated into $Ce_{0.5}Zr_{0.5}O_2$ lattice. This is evident from the increase in the lattice parameter of $Ce_{0.5}Zr_{0.5}O_2$ from a=5.323(2) Å to a=5.343(4) Å (Table 1). Apparently, Ni^{2+} cations replace a part of Ce^{4+} and Zr^{4+} ions in the surface layers of nanodomains, which is accompanied by the increase of concentration of oxygen vacancies. The occupancy of oxygen position in the fluorite structure decreases from 0.96 to 0.91. Moreover, the average crystallite size decreases from 8-10 nm to 7-9 nm, and strains increase from 0.27 to 0.29. It means that incorporation of Ni cations leads to the additional disordering of fluorite-like structure. The average crystallite size of NiO nanoparticles detected by XRD is about 10-14 nm, strains density is about 0.13.

Full-profile Rietveld refinement for the 5%Ni/$Ce_{0.7}Zr_{0.3}O_2$ sample is shown in Figure 4. NiO content estimated by Rietveld analysis is also about 6 weight %. As opposite to the previous case, the lattice constant of $Ce_{0.7}Zr_{0.3}O_2$ decreases from a=5.337 (8) Å to a=5.3222(4) Å (Table 1) for the Ni-doped sample. Occupancy of oxygen position is exactly 1.00. The average crystallite size is 7-9 nm and strains density is 0.32. The average crystallite size of NiO is about 9-13 nm, strains are almost absent. This suggests that for Ce-Zr-O support with a high content of Ce incorporation of Ni cations into the surface layers of complex domains is less pronounced which can be tentatively explained by their lesser disordering [22].

3.1.2 TEM

As follows from TEM data (Figs. 5-8), Ce-Zr-O mixed oxides are comprised of stacked nanodomains with typical sizes ~ 5-10 nm, which agrees with XRD data. Their boundaries are disordered, which explains a high density of microstrains estimated by Rietveld analysis (Table 1). Observed variation of the (111) fluorite distance from 3.09 to 3.11 Å (Fig. 5) is moderate agreeing with a reasonable uniformity of elements distribution between and within domains.

Table 1: Refined unit cell parameters, volumes and average crystallite sizes and strains.

Sample	Unit cell parameters and volumes Ce-Zr-O	Average crystallite sizes Ce-Zr-O (Strains)	Unit cell parameters NiO	Average crystallite sizes Ni-O (Strains)
$Ce_{0.5}Zr_{0.5}O_2$	Cubic a=5.3236(3) Å V=150.87(2) Å^3	8-10 nm (0.27)	-	-
$Ce_{0.5}Zr_{0.5}O_2$	Tetragonal t' a_F = 5.317(1) Å c = 5.32(2) Å V = 150.8 Å^3	8-10 nm (0.27)	-	-
5%Ni/$Ce_{0.5}Zr_{0.5}O_2$	Cubic a=5.3428(4) Å V=152.51(4) Å^3	7-9 nm (0.29)	a=4.181(2) Å	10-14 nm (0.13)
5%Ni/$Ce_{0.7}Zr_{0.3}O_2$	Cubic a=5.3222(4) Å V=150.76(4) Å^3	7-9 nm (0.32)	a=4.179(2) Å	9-13 nm (0.00)

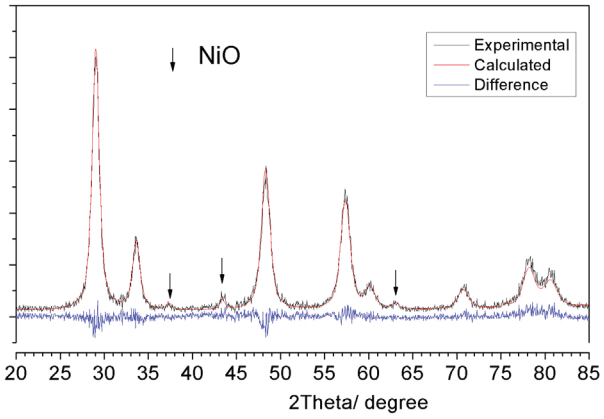

Figure 3: Full-profile Rietveld refinement for 5%Ni/$Ce_{0.5}Zr_{0.5}O_2$ sample.

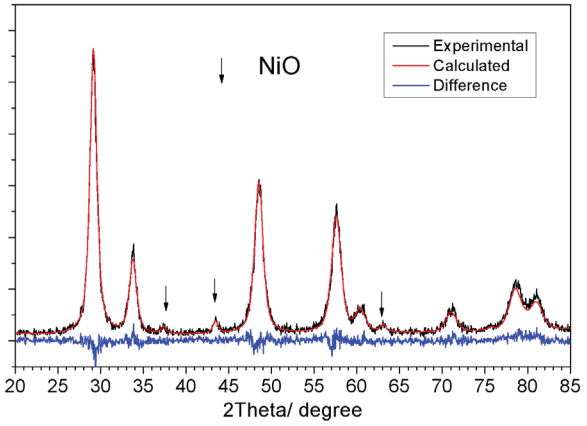

Figure 4: Full-profile Rietveld refinement for the 5%Ni/$Ce_{0.7}Zr_{0.3}O_2$ sample.

Elemental mapping (Fig. 6) demonstrates rather uniform distribution of Ce and Zr between nanodomains which does not exclude some variation in the second coordination spheres of these cations within domains. Supported Ni is also distributed rather uniformly (Fig. 6) both in the form of epitaxial NiO layers on the surface of support domains with NiO (110) planes clearly resolved (Fig. 7) as well as separate NiO nanoparticles with the same orientation (Fig. 8).

3.1.3 Raman

As follows from analysis of data shown in Fig. 9, for Ce-Zr-O oxides prepared in this work, Raman spectra correspond to a cubic phase even for a sample with Ce/Zr ratio 1. Here, the band at 470 cm^{-1} is due to the triply degenerate F2g mode; a weak band at~ 600 cm^{-1} corresponds to a non-degenerate longitudinal optical mode of CeO_2 observed due to lattice defects breaking selection rules (oxygen vacancies, etc). Displacement of the oxygen atoms from their ideal fluorite lattice positions due to Zr^{4+} incorporation results in the appearance of a weak band at ~300 cm^{-1} [6, 25, 26].

Broadening of the main peak at ~ 470 cm^{-1} for $Ce_{0.5}Zr_{0.5}O_2$ sample apparently reflects a higher disordering of its local structure caused by incorporation of Zr into the fluorite –like lattice [6, 25, 26]. However, a peak at ~ 600 cm^{-1} for this sample is less pronounced as compared with that for samples prepared either by Pechini route with water solutions [27], surfactant-assisted route [6] or mild urea hydrolysis based hydrothermal method [26]. This suggests a higher total disordering of the structure of samples prepared in this work probably caused by their higher hydroxylation and hydration (see XRD data above).

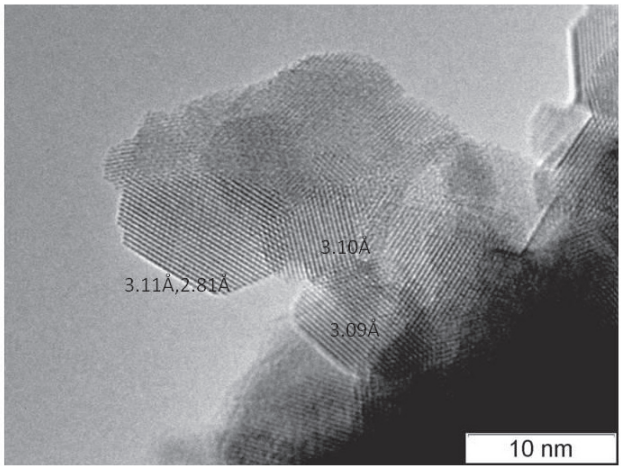

Figure 5: Typical high resolution TEM image of nanodomains in $Ce_{0.5}Zr_{0.5}O_2$ sample.

3.1.4 UV-Vis DR spectra

For Ce-Zr-O mixed oxides UV-Vis spectral features (not shown for brevity) were very close to those earlier observed [6, 27]. In the UV range they are determined by superposition of bands corresponding to charge transfer from O^{2-} to Ce^{4+} (maximum at ~33000 cm^{-1}), to Ce^{3+} (maximum at ~ 38000 cm^{-1}) and to Zr^{4+} (maximum at ~ 48000 cm^{-1}) cations. With the increase of Zr content the relative intensity of O^{2-}-Ce^{3+} band was increased reflecting the increase of the oxide lattice disordering [6, 16].

UV-Vis DR spectral features observed for Ni-loaded Ce-Zr-O (Fig. 10a) were determined by superposition of bands corresponding to mixed oxides, NiO (Fig. 10b) and Ni^{2+} cations in the surface layer of ceria-zirconia supports (band at ~ 13800 cm^{-1}).

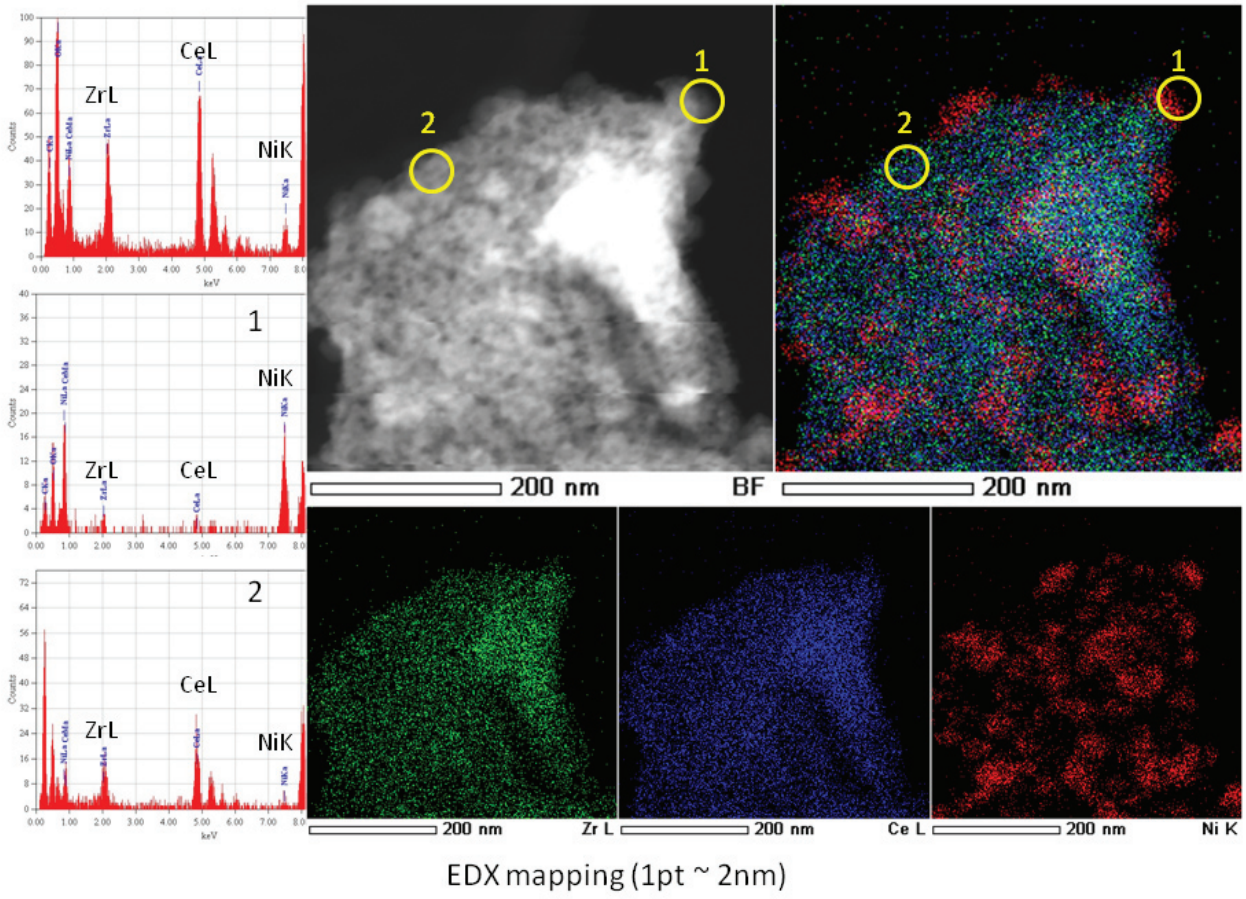

Figure 6: Elemental mapping for $5Ni/Ce_{0.5}Zr_{0.5}O_2$ sample.

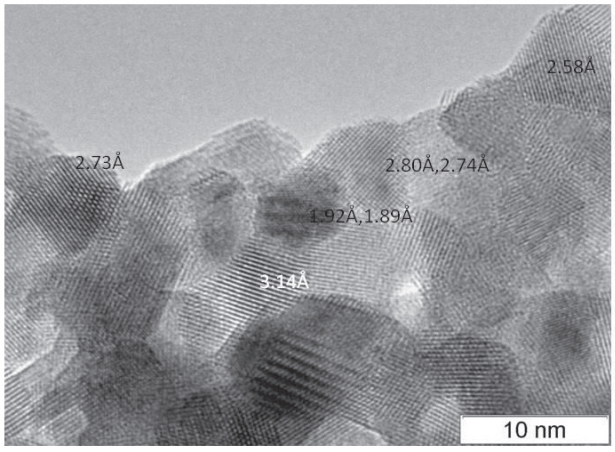

Figure 7a: Typical high resolution TEM image of nanodomains in 5Ni/$Ce_{0.5}Zr_{0.5}O_2$ sample.

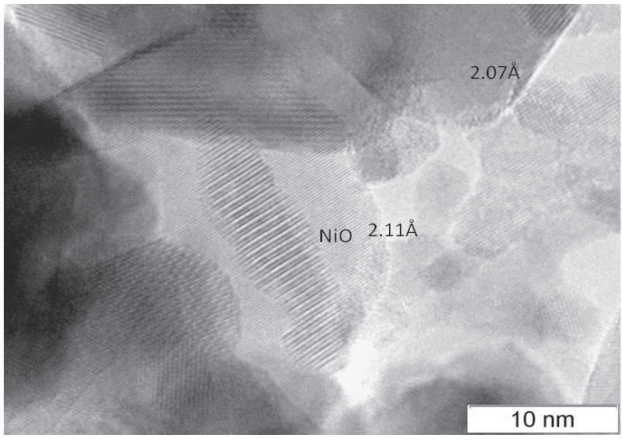

Figure 7b: Typical high resolution TEM image of nanodomains in 5Ni/$Ce_{0.7}Zr_{0.3}O_2$ sample.

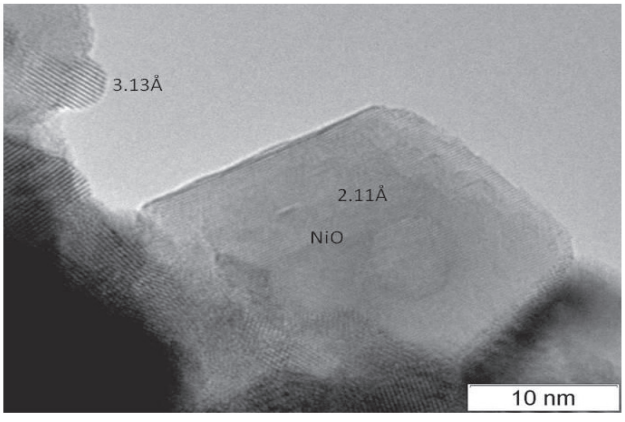

Figure 8: Typical high resolution TEM image of separate NiO nanoparticle in 5Ni/$Ce_{0.5}Zr_{0.5}O_2$ sample.

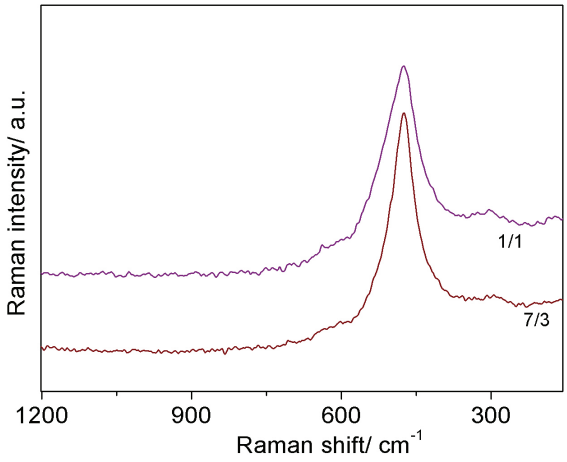

Figure 9: Raman spectra of Ce-Zr-O samples with Ce/Zr ratio 1/1 and 7/3.

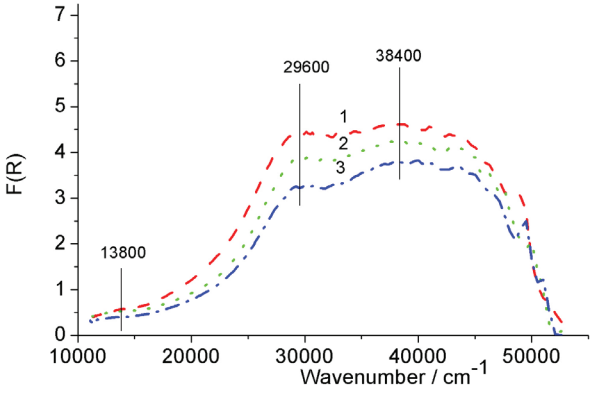

Figure 10a: UV-Vis spectra of Ni-loaded Ce-Zr-O oxides. 1– 5Ni/$Ce_{0.3}Zr_{0.7}O_2$; 2 – 5Ni/$Ce_{0.5}Zr_{0.5}O_2$; 3 – 5Ni/$Ce_{0.7}Zr_{0.3}O_2$.

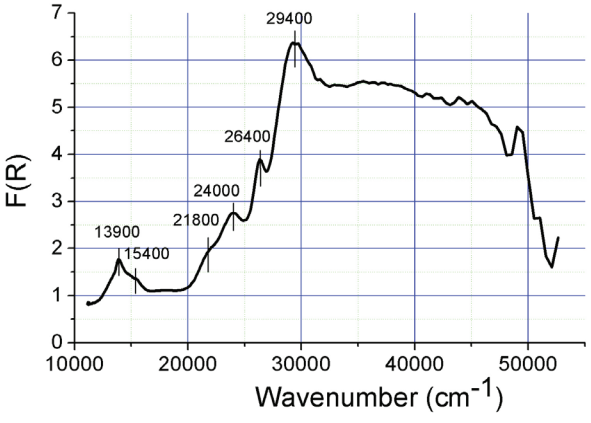

Figure 10b: reference UV-Vis spectrum of NiO oxide calcined at 900 °C.

Apparent shift of the absorption edge with the Zr content in complex oxide support reflects both an increase of Ce^{3+} content [27] as well as more facile incorporation of Ni^{2+} cations into the surface layer of mixed oxides leading to their expansion (vide supra XRD data).

3.2 Surface properties

3.2.1 XPS

Figure 11 presents Zr3d spectrum of 5% $Ni/Ce_{0.5}Zr0_{.5}O_2$ sample. This spectrum is well fitted by a doublet $Zr3d_{5/2}$ – $Zr3d_{3/2}$ with the components integral intensity ratio equal to 3 : 2. The difference between $Zr3d_{5/2}$ – $Zr3d_{3/2}$ levels determined by the spin-orbital splitting is equal to 2.39 eV. E_B of $Zr3d_{5/2}$ for sample before and after reaction is equal to 182.05 eV (Fig. 11, Table 2), which corresponds to zirconium in Zr^{4+} state. For stoichiometric ZrO_2 E_B of $Zr3d_{5/2}$ is in the range of 182.2-183.3 eV [28-31].

XPS spectra of Ce*3d* are shown in Fig. 12. These spectra have a very complex shape due to both spin-orbital splitting as well as presence of Ce in 3+ and 4+ states [6, 32, 33]. First, Ce 3d level is splitted into $Ce3d_{5/2}$ и $Ce3d_{3/2}$ doublet with the ratio of the integral intensity of lines as 3:2. Second, each component of doublet is splitted into three lines for CeO_2 (v/u, v″/u″, v‴/u‴) or two lines for Ce_2O_3 (v′/u′, v_0/u_0). Analysis of the spectra deconvolution into the individual components revealed that a share of Ce^{4+} is ~ 60% (Table 3).

$Ni2p_{3/2}$ spectra of studied catalysts (Fig. 13) are comprised of the main peak at 853.5 eV and intense peaks of shake-up satellites at 855.4 and 861.1 eV. These satellites caused by the multielectron processes [34- 37] are typical for Ni^{2+} compounds, such as NiO, $Ni(OH)_2$, $NiSiO_3$ etc [38-43], while being absent for Ni^0 and Ni^{3+} compounds [36]. After testing in CH_4 DR reaction Ni is also present in the metallic state (E_B 852.3 eV, the relative amount up to 30% , Table 2), which is accompanied by some aggregation of Ni (Table 3).

3.2.2 FTIRS of adsorbed CO

Pretreatment in O_2. For ceria-zirconia samples, at the lowest surface CO coverage, the bands at ~ 2135 and ~ 2185 cm^{-1} with comparable intensity are observed. While the former band corresponds to CO complexes with Ce^{3+} species, the latter one can be assigned to carbonyl complexes of Zr^{4+} such as those observed after CO adsorption at 77 K on the surface of stabilized zirconia samples [27, 45]. A higher

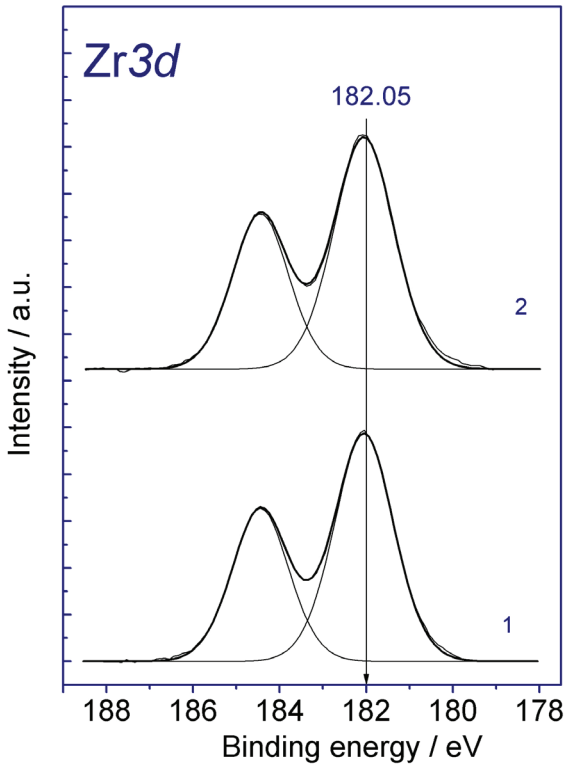

Figure 11: Zr3d spectra for 5%$Ni/Ce_{0.5}Zr_{0.5}O_2$ sample as prepared (1) and after testing in CH_4 DR (2).

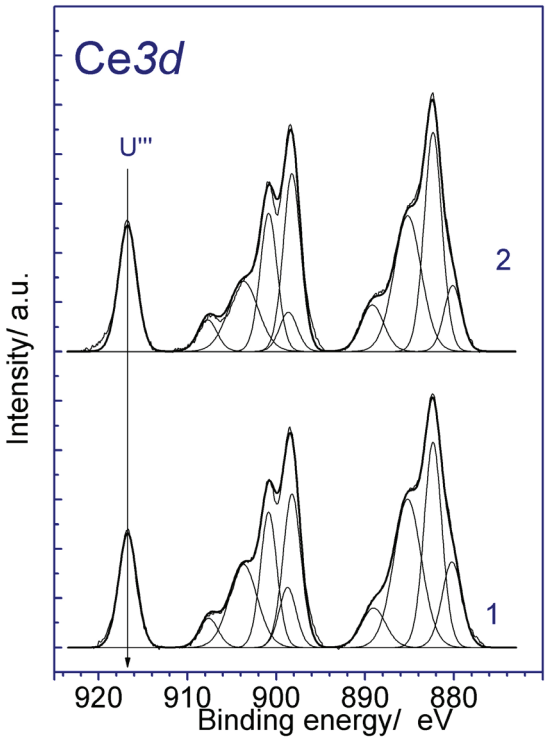

Figure 12: Ce*3d* spectra for 5%Ni/ $Ce_{0.5}Zr_{0.5}O_2$ sample as prepared (1) and after testing in CH_4 DR (2).

Table 2: Binding energies of Zr$3d_{5/2}$, Ce$3d_{3/2}$-u''', O1*s* и Ni$2p_{3/2}$ (eV).

№	Sample	Zr$3d_{5/2}$	Ce$3d_{3/2}$ u'''	Ni$2p_{3/2}$, %	O1*s*	C1*s*
1	Fresh	182.1	916.7	853.6	529.6 531.7	284.8
2	After testing	182.1	916.8	852.2 (28) 853.6 (72)	529.5 531.5	

Table 3: Atomic ratio of elements in the surface layers.

№	Sample	[Ce]/[Zr]	[Ni]/[Zr+Ce]	[O]/[Zr+Ce]	[C]/[Zr+Ce]	Ce^{4+}, %
1	Fresh	1.52	0.143	2.29	1.34	57
2	After testing	1.45	0.066	2.26	1.12	64

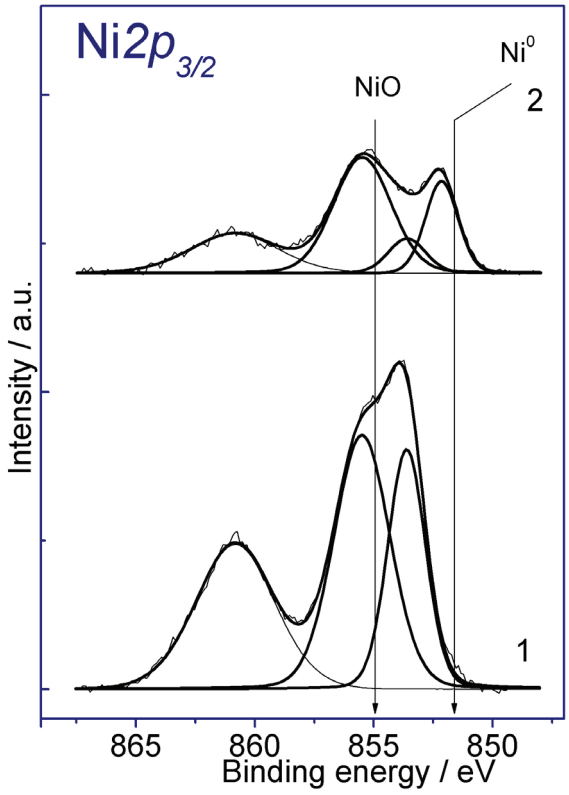

Figure 13: Ni$2p_{3/2}$ spectra for 5%Ni/ $Ce_{0.5}Zr_{0.5}O_2$ sample as prepared (1) and after testing in CH_4 DR (2).

frequency of Zr^{4+} -CO band position indicates a higher acidity of corresponding Lewis acid site as compared with that for Ce^{4+}.

In spectra of Ni-loaded samples pretreated in O_2, a band at 2150-2170 cm^{-1} is observed (Fig. 14), which can be assigned to CO adsorbed on surface hydroxyls, cations of support as well as to CO complexes with Ni^{2+} cations. A band at 2135 cm^{-1} can be assigned to physisorbed CO. Bands at 2110 cm^{-1} and ~ 2080 cm^{-1} can be assigned to CO adsorption on Ni^{+} cations and Ni^{0} sites appeared due to reduction of reactive clustered Ni^{2+} -O surface species at CO adsorption [46, 47]. After heating the sample from 77K to room temperature, the absorption band disappears without appearance of any bands corresponding to CO adsorption on Ni metal sites [49,50].

Pretreatment in H_2. Figure 15 shows IR spectra of CO adsorbed after pretreatment in H_2 on 2%Ni/$Ce_{0.5}Zr_{0.5}O_2$ sample. The bands at 2150-2180 cm^{-1} correspond to CO adsorption on surface hydroxyls and cations of support. A band at 2115 cm^{-1} is assigned to Ni^{+} -CO carbonyls, while the bands at 2047 and 2080 $см^{-1}$ correspond to CO adsorption on the metal Ni sites.

In the spectra of CO adsorption at room temperature (Fig. 16), the bands corresponding to bridging and terminal carbonyls of Ni^{0} are observed. The bands with wavenumber below 2000 cm^{-1} are attributed to bridging carbonyls (Ni^{0}-CO-Ni^{0}) while the bands at 2000-2100 cm^{-1} refer to terminal carbonyls (Ni^{0}-CO). Table 4 presents concentrations of respective complexes for samples with different Ce/Zr ratio estimated from the integral intensities of characteristic absorption bands using the integral coefficients of absorption [51].

In general, the highest amount of terminal carbonyls corresponding to CO adsorption on Ni atoms not having the nearest neighbor Ni atom to form the bridging complex is observed for 2Ni/$Ce_{0.5}Zr_{0.5}O_2$ sample with the highest disordering of support (vide supra), thus favoring strong metal-support interaction (incorporation of Ni cations into the support layer, decoration of NiO particles by support species, etc), which is required to prevent coking and sintering [13, 16, 19]. The total surface concentration of accessible Ni sites amounts up to 4% of monolayer.

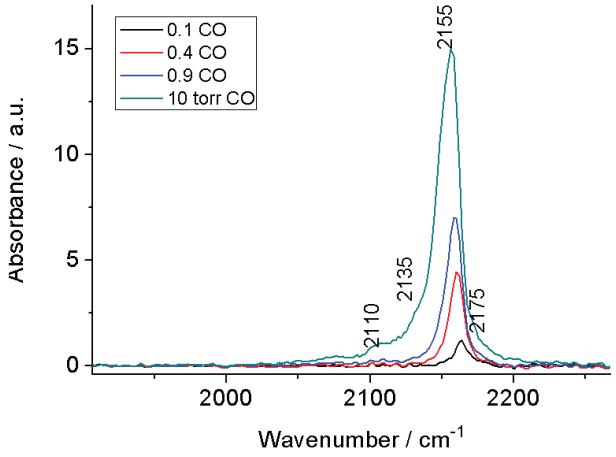

Figure 14: Differential IR spectra of CO adsorbed on 2%Ni/$Ce_{0.5}Zr_{0.5}O_2$ sample (after O_2 pretreatment) at 77 K and CO pressure of 0.1-10 Torr.

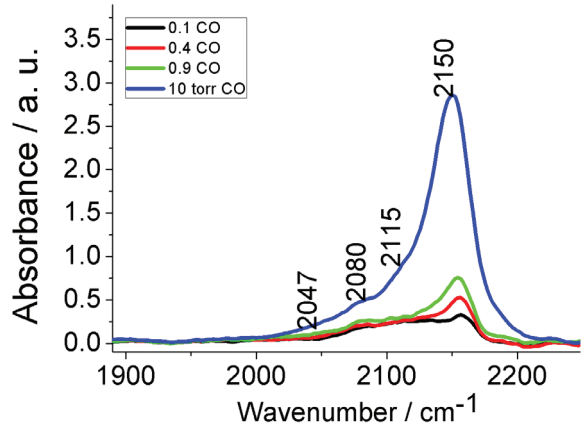

Figure 15: FTIR spectra of CO adsorbed after pretreatment in H_2 on 2Ni/$Ce_{0.5}Zr_{0.5}O_2$ sample at 77 K and CO pressure of 0.1-10 Torr.

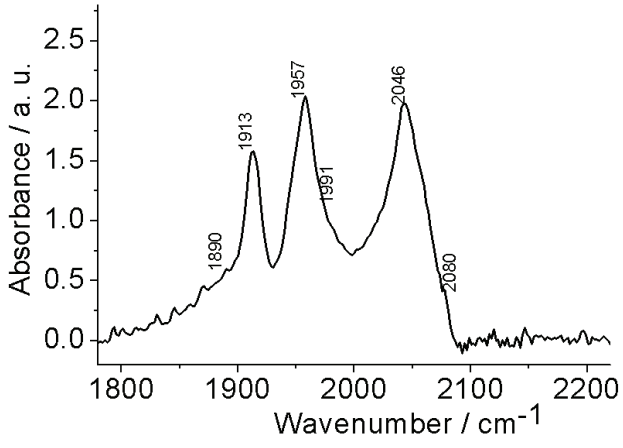

Figure 16: FTIR spectrum of CO adsorbed after pretreatment in H_2 on 2Ni/$Ce_{0.5}Zr_{0.5}O_2$ sample at room temperature and CO pressure of 10 Torr.

This is close to the surface concentration of Ni estimated by XPS (7-10% monolayer) with a due regard for a lower concentration of Ni (2%) in samples studied by FTIRS.

3.3 Reactivity

For mixed $Ce_{0.5}Zr_{0.5}O_2$ oxide prepared via a traditional Pechini route [27] as well as samples prepared by other routes (citrate, etc [25, 52]) and characterized by moderate (~ 30 m^2/g) BET specific surface area, H_2 TPR of the surface starts at ~ 300 °C followed by bulk reduction characterized by one maximum at ~ 600 °C and diffusion plateau at higher temperatures [25, 27]. This is explained by a high lattice oxygen mobility in these mixed oxides, so the total reduction is controlled by the surface reaction [27]. Note, however, that for high (up to 180 m^2/g according to BET) surface area $Ce_{0.6}Zr_{0.4}O_2$ samples prepared via template-assisted route [6] as well as for $Ce_{0.5}Zr_{0.5}O_2$ citrate sample with the BET surface area ~ 40 m^2/g mildly reoxidized after severe reduction [52], the surface and bulk H_2 TPR processes were found to be presented by two overlapping broad peaks with maxima situated at ~600 °C and 900 °C [6], or ~ 400 and 600 °C [52], respectively.

For Ni-loaded samples reduction process is apparently shifted to lower temperature (Fig. 17) due to fast reduction of small clustered Ni-O species (a shoulder at ~ 200 °C), epitaxial NiO layers and separate NiO particles (peaks at ~300 and ~ 400 °C) followed by H_2 molecules activation on Ni metal sites and fast H atoms spillover to the oxide surface accelerating its reduction [27]. Note that as dependent upon the real/defect structure of NiO particles and their interaction with support, their H_2 TPR maximum can be situated in the range of 300-450 °C [6, 53], so enhanced low-temperature reducibility of 5Ni/$Ce_{0.5}Zr_{0.5}O_2$ sample can be explained only by enhanced reactivity of clustered Ni-O surface species. For 5Ni/$Ce_{0.6}Zr_{0.4}O_2$ samples prepared via template-assisted route [6] even surface reduction was presented by two H_2 TPR peaks situated at ~450 and 750 °C, implying very strong NiO-support interaction [6] apparently resulting in a low reactivity of supported NiO particles.

3.4 Catalytic properties

Even in diluted (1% CH_4 +1%CO_2 in He) reaction mixture 5Ni/$Ce_{0.5}Zr_{0.5}O_2$ the sample prepared in this work and pretreated in O_2 was reduced by the reaction feed in the temperature-programmed mode starting from ~600 °C, thus demonstrating noticeable activity in CH_4 DR. With

Table 4: Concentration of different types of Ni^0 centers by FTIRS of adsorbed CO data.

Sample	νCO, см$^{-1}$	Concentration of sites, ⌈mol/g	Content of bridging carbonyls, ⌈mol/g	Content of terminal carbonyls, ⌈mol/g
$2Ni/Ce_{0.7}Zr_{0.3}O_2$	1895	15		
	1913	3		
	1958	5	33	12
	1981	10		
	2047	11		
	2067	0.6		
$2Ni/Ce_{0.5}Zr_{0.5}O_2$	1890	7		
	1913	2		
	1957	3	17	21
	1991	5		
	2046	7		
	2080	14		
$2Ni/Ce_{0.3}Zr_{0.7}O_2$	1915	8		
	1953	4		
	1980	9	21	9
	2034	4		
	2057	5		

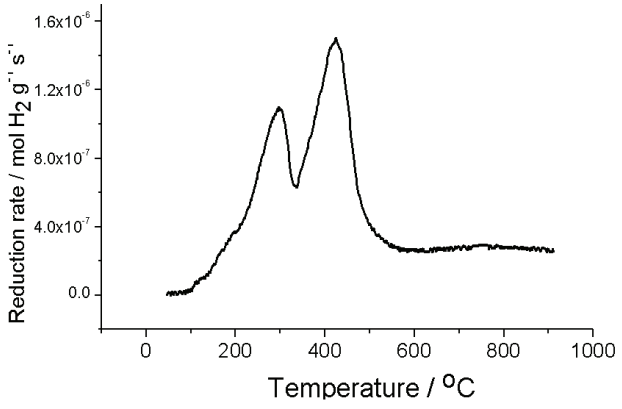

Figure 17: H_2 TPR spectrum for $5Ni/Ce_{0.5}Zr_{0.5}O_2$ sample.

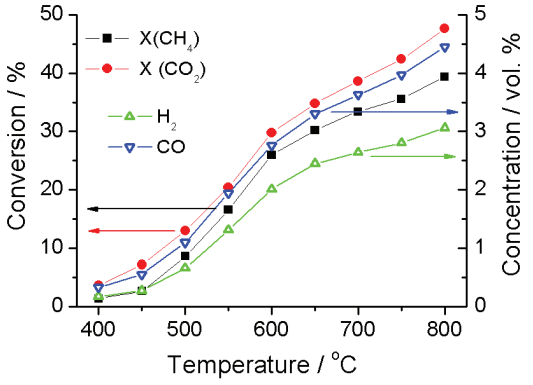

Figure 18a: Temperature dependence of reagents conversions and products concentrations for $5Ni/Ce_{0.5}Zr_{0.5}O_2$ catalyst in feed 5% CH_4 + 5% CO_2 in He. Contact time 8 ms, pretreatment 1 h at 400 °C in O_2 followed by 1h at 400 °C in 10% H_2 in He.

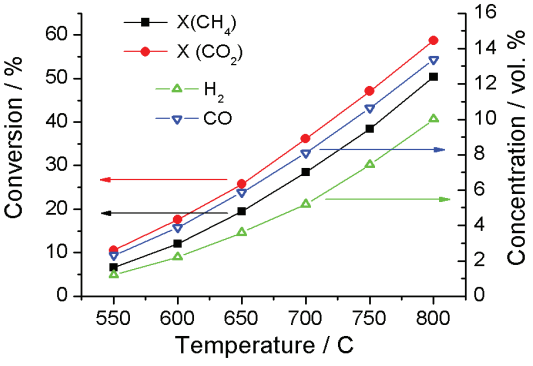

Figure 18b: Temperature dependence of reagents conversions and products concentrations for $5Ni/Ce_{0.5}Zr_{0.5}O_2$ catalyst in feed 15% CH_4 + 15% CO_2 in N_2. Contact time 8 ms, pretreatment 1 h at 400 °C in O_2, activation in reaction feed at 400 °C.

each step-wise increase in temperature activity first increased then slowly decreased due to apparent sintering of the active components with temperature as follows from XPS data (vide supra). However, in this diluted feed even at short (8 ms) contact times CH_4 conversion achieved equilibrium values (>90%) at 800 °C, performance was stable with time-on-stream at this temperature as well as in the course of step-wise decreasing the temperature to 400-500 °C. For more concentrated feeds (5-15% CH_4, CO_2/CH_4=1) conversions of reagents were lower due to apparent not first-order kinetics [54] (Fig. 18).

Slightly lower reagents conversions for less concentrated feed with 5% of CH_4 are explained by more tough reducing pretreatment in H_2 resulting in a higher sintering of supported Ni.

Estimation of the efficient first-order specific rate constant at 800 °C from the value of CH_4 conversion ~ 50%

in frames of the plug-flow reactor model and specific surface area ~ 50 m^2/g gives value ~ 2 $s^{-1}m^{-2}$, which is much higher than specific rate constants earlier obtained for NiO-loaded mixed ceria-zirconia oxide doped by Pr and prepared via traditional Pechini route (~ 0.2 $s^{-1}m^{-2}$) [11]. For the latter catalysts, a low activity was due to blocking the surface of Ni particles by amorphous carbon layers in agreement with similar results obtained by Roh et al. for Ni/CeO_2 or Ni/ZrO_2 [8]. Hence, apparent non-uniformity of Ce and Zr distribution between domains of mixed Ce-Zr-O oxide prepared via traditional Pechini route causes deactivation of supported Ni due to carbon deposition. A high level of activity ($k_{eff.}$ ~2-3 $s^{-1}m^{-2}$ at 800 °C) and coking stability were obtained for catalysts based on Ce-Zr-O oxides prepared via traditional Pechini route only by depositing Ni+Ru or complex perovskite-like precursors such as $LaNi(Pt,Ru)O_3$, which helps to prevent coking by decoration of the surface layer of Ni nanoparticles by LaO_x species as well as formation of surface Ni-Ru alloy layers less prone to coking due to Ni atoms ensemble dilution effect [11, 55, 56]. Efficient activation of CO_2 molecules on the reduced sites of Ce-Zr-O complex oxides and fast diffusion of thus formed reactive oxygen species to the metal-support interface where they consume coke precursors $-CH_x$ species also play important role in preventing coking [55, 56]. Hence, modification of Pechini preparation procedure by dissolving metal salt directly in ethylene glycol allowed to provide a higher activity and coking stability of Ni-loaded catalysts even without such additives as Ru or LaO_x, though in any case it will be of both fundamental and practical interest to check their effect in further studies. TEM studies of catalysts after testing demonstrated absence of any amorphous carbon layers as well as filaments.

4 Conclusions

Modification of Pechini route of mixed Ce-Zr-O oxides preparation by using ethylene glycol solutions of metal salts instead of aqueous ones allowed to obtain nanocrystalline disordered cubic phase with a high spatial uniformity of elements distribution between domains and their surface and bulk up to Ce/Zr ratio =1. Such a disordering provides a strong interaction between loaded by wet impregnation NiO and support manifested in a partial incorporation of Ni cations into the surface layers of Ce-Zr-O domains stabilizing their high dispersion and reactivity as epitaxial NiO layers in as-prepared catalysts, then transformed into stable to sintering Ni clusters and surface layers in reaction conditions. Such a stabilization along with a high mobility of the lattice oxygen of Ce-Zr-O support provides high activity and coking stability of thus developed catalysts of methane dry reforming.

Conflict of interest: The authors declare that there is no conflict of interest regarding the publication of this paper.

Acknowledgements: Support by NICE project of ERA Net Rus Plus Call and Russian Ministry of Education and Science under related contract №14.616.21.0036 is gratefully acknowledged

References

[1] Shah Ya. T. and Gardner T. H., Dry reforming of hydrocarbon feedstocks, Catal. Rev., 2014, 56, 476-536.

[2] Verykios X. E., Catalytic dry reforming of natural gas for the production of chemicals and hydrogen, Int. J. Hydrogen Energ., 2003, 28, 1045-1063.

[3] Swaan H. M., Kroll V. C. H., Martin G.A., and Mirodatos C., Deactivation of supported nickel catalysts during the reforming of methane by carbon dioxide, Catal. Today, 1994, 21, 571-578.

[4] Pakhare D. and Spivey J., A review of dry (CO_2) reforming of methane over noble metal catalysts, Chem. Soc. Rev., 2014, 43, 7813-7837.

[5] Roh H.-S., Potdar H.S., Jun K.-W., Kim J.-W., and Oh Y.-S., Carbon dioxide reforming of methane over Ni incorporated into $Ce–ZrO_2$ catalysts, Appl. Catal. A-Gen., 2004, 276, 231–239.

[6] Sukonket T., Khan A., Saha B., Ibrahim H., Tantayanon S., Kumar P., et al., Influence of the catalyst preparation method, surfactant amount, and steam on CO_2 reforming of CH_4 over $5Ni/Ce_{0.6}Zr_{0.4}O_2$ Catalysts, Energ. Fuel., 2011, 25, 864–877.

[7] Kambolis A., Matralis H., Trovarelli A., and Papadopoulou Ch., Ni/CeO_2-ZrO_2 catalysts for the dry reforming of methane, Appl. Catal. A-Gen., 2010, 377, 16–26.

[8] Roh H.-S., Potdar H. S., and Jun K.-W., Carbon dioxide reforming of methane over co-precipitated $Ni–CeO_2$, $Ni–ZrO_2$ and $Ni–Ce–ZrO_2$ catalysts, Catal. Today, 2004, 93–95, 39–44.

[9] Damyanova S., Pawelec B., Arishtirova K., Martinez Huerta M.V., and Fierro J. L. G., The effect of CeO_2 on the surface and catalytic properties of $Pt/CeO_2–ZrO_2$ catalysts for methane dry reforming, Appl. Catal. B-Environ., 2009, 89, 149–159.

[10] Sadykov V.A., Gubanova E.L., Sazonova N.N., Pokrovskaya S.A., Chumakova N.A., Mezentseva N.V., et al., Dry reforming of methane over Pt/PrCeZrO catalyst: kinetic and mechanistic features by transient studies and their modelling, Catal. Today, 2011, 171, 140–149.

[11] Sadykov V., Mezentseva N., Zevak E., Bobin A., Krieger T., Gulayev R., et al., Nanocrystalline doped ceria-zirconia solid solutions promoted by Pt and/or Ni: structure, surface properties and catalytic performance in reactions of syngas production, in: First International Conference on Materials for Energy (4-8 July 2010, Karlsruhe, Germany), Extended Abstracts - Book B, Dechema, 2010, 845–847.

[12] Liotta L. F., Pantaleo G., Macaluso A., Marci G., Gialanella S., Deganello G., Ceria-zirconia nanostructured materials for catalytic applications: textural characteristics and redox properties, J. Sol-Gel Sci. Techn. 2003, 28, 119–132.
[13] Sadykov V., Usoltsev V., Yeremeev N., Mezentseva N., Pelipenko V., Krieger T., et al., Functional nanoceramics for intermediate temperature solid oxide fuel cells and oxygen separation membranes, J. Eur. Ceram. Soc., 2013, 33, 2241–2250.
[14] Kolko V. P., Kriventsov V. V., Kochubey D. I., Zyuzin D. A., Moroz E. M., Sadykov V. A., et al., Structural determination of ceria–zirconia nanosystem doped by Gd, Nucl. Instrum. Meth. A, 2007, 575, 91–95.
[15] Scofield J. H., Hartree-Slater subshell photoionization cross-sections at 1254 and 1487 eV, J. Electron Spectrosc., 1976, 8, 129–137.
[16] Kapokova L., Pavlova S., Bunina R., Alikina G., Krieger T., Ishchenko V., et al., Dry reforming of methane over $LnFe_{0.7}Ni_{0.3}O_{3-x}$ perovskites: Influence of Ln nature, Catal. Today, 2011, 164, 227–233.
[17] Di Monte R. and Kašpar J., Nanostructured CeO_2–ZrO_2 mixed oxides, J. Mater. Chem., 2005, 15, 633–648.
[18] Abniyaz A., Watanabe T., and Yoshimura M., Tetragonal Nanocrystals from the $Zr_{0.5}Ce_{0.5}O_2$ Solid solution by hydrothermal method, J. Phys. Chem. B, 2005, 109, 6136–6139.
[19] Sadykov V. A., Kriventsov V. V., Moroz E. M., Borchert Y. V., Zyuzin D. A., Kol'ko V. P., et al., Ceria-zirconia nanoparticles doped with La or Gd: effect of the doping cation on the real structure, Solid State Phenom., 2007,128, 81–88.
[20] Mamontov E., Brezny R., Koranne M., and Egami T., Nanoscale heterogeneities and oxygen storage capacity of $Ce_{0.5}Zr_{0.5}O_2$, J. Phys. Chem. B, 2003, 107, 13007–13014.
[21] Alifanti M., Baps B., Blangenois N., Naud J., Grange P., and Delmon B., Characterization of CeO_2-ZrO_2 mixed oxides. Comparison of the citrate and sol-gel preparation methods, Chem. Mater., 2003, 15, 395–403.
[22] Mamontov E., Egami T., Brezny R., Koranne M., and Tyagi S., Lattice defects and oxygen storage capacity of nanocrystalline ceria and ceria–zirconia, J. Phys. Chem. B, 2000, 104, 11110–11116.
[23] Sadykov V.A., Mezentseva N., Alikina G., Lukashevich A., Muzykantov V., Kuznetsova T., et al., Nanocrystalline doped ceria-zirconia fluorite-like solid solutions promoted by Pt: structure, surface properties and catalytic performance in syngas generation, Mater. Res. Soc. Symp. P. (MRS Proceedings), 2007, 988, pp. QQ06-04.1-6. DOI: 10.1557/PROC-988-0988-QQ06-04.
[24] Sadykov V., Mezentseva N., Alikina G., Lukashevich A., Muzykantov V., Bunina R., et al., Doped nanocrystalline pt-promoted ceria-zirconia as anode catalysts for IT SOFC: Synthesis and properties, Mater. Res. Soc. Symp. P. (MRS Proceedings), 2007, 1023, pp. JJ02-07.1-6. DOI: 10.1557/PROC-1023-JJ02-07.
[25] Vidal H., Kašpar J., Pijolat M., Colon G., Bernal S., Cordon A., et al, Redox behavior of CeO_2-ZrO_2 mixed oxides: II. Influence of redox treatment on low surface area catalysts, Appl. Catal. B-Environ., 2001, 30, 75–85.
[26] Si R., Zhang Ya-W., Li S.-J., Lin B.-X., and Yan Ch.-H., Urea-based hydrothermally derived homogeneous nanostructured $Ce_{1-x}Zr_xO_2$ (x=0-0.8) solid solutions: A strong correlation between oxygen storage capacity and lattice strain, J. Phys. Chem. B, 2004, 108, 12481–1248, 2004.
[27] Sadykov V. A., Kuznetsova T. G., Alikina G. M., Frolova Yu. V., Lukashevich A. I., Muzykantov V. S., et al., Chapter 5. Ceria-based fluorite-like oxide solid solutions promoted by precious metals as catalysts of methane transformation into syngas, in: McReynolds D.K. (Ed.) New Topics in Catalysis Research, Nova Science Publishers, New York, 2007.
[28] Tsunekawa S., Asami K., Ito S., Yashima M., and Sugimoto T., XPS study of the phase transition in pure zirconium oxide nanocrystallites, Appl. Surf. Sci., 2005, 252, 1651–1656.
[29] Jeon T. S., White J.M., and Kwong D. L., Thermal stability of ultrathin ZrO_2 films prepared by chemical vapor deposition on Si(100) , Appl. Phys. Lett., 2001, 78, 368–370.
[30] Kim M.-S., Ko Y.-D., Hong J.-H., Jeong M.-C., Myoung J.-M., and Yun I., Characteristics and processing effects of ZrO_2 thin films grown by metal-organic molecular beam epitaxy, Appl. Surf. Sci., 2004, 227, 387–398.
[31] Barr T. L., An ESCA study of the termination of the passivation of elemental metals, J. Phys. Chem., 1978, 82, 1801–1810.
[32] Borchert H., Frolova Y.V., Kaichev V.V., Prosvirin I.P., Alikina G.M., Lukashevich A.I., et al., Electronic and chemical properties of nanostructured cerium dioxide doped with praseodymium, J. Phys. Chem. B, 2005, 109, 5728–5738.
[33] Christou S. Y., Álvarez-Galván M. C., Fierro J. L. G., and Efstathiou A. M., Suppression of the oxygen storage and release kinetics in $Ce_{0.5}Zr_{0.5}O_2$ induced by P, Ca and Zn chemical poisoning, Appl. Catal. B-Environ., 2011, 106, 103–113.
[34] Alders D., Voogt F. C., Hibma T., and Sawatzky G. A., Nonlocal screening effects in 2p X-ray photoemission spectroscopy of NiO (100), Phys. Rev. B, 1996, 54, 7716–7719.
[35] Van Veenendaal M. A. and Sawatzky G.A., Nonlocal screening effects in 2p X-ray photoemission spectroscopy core-level line shapes of transition metal compounds, Phys. Rev. Lett., 1993, 70, 2459–2462.
[36] Carley A. F., Jackson S. D., O'Shea J. N., and Roberts M. W., The formation and characterization of Ni^{3+} - an X-ray photoelectron spectroscopic investigation of potassium-doped Ni(110)-O, Surf. Sci., 1999, 440, L868–L874.
[37] Dube C. E., Workie B., Kounaves S. P., Rabbat A., Aksu M. L., and Davies G., Electrodeposition of metal alloy and mixed oxide films using a single precursor tetranuclear copper nickel complex, J. Electrochem. Soc., 1995, 142, 3357–3365.
[38] Kosova N. V., Devyatkina E. T., and Kaichev V. V., Mixed layered Ni-Mn-Co hydroxides: Crystal structure, electronic state of ions, and thermal decomposition, J. Power Sources, 2007, 174, 735–740.
[39] Li C. P., Proctor A., and Hercules D. M., Curve Fitting Analysis of ESCA Ni 2p Spectra of Nickel-Oxygen Compounds and Ni/Al_2O_3 Catalysts, Appl. Spectrosc., 1984, 38, 880–886.
[40] Lorenz P., Finster J., Wendt G., Salyn J. V., Zumadilov E. K., and Nefedov V. I., ESCA investigations of some NiO/SiO_2 and $NiO-Al_2O_3/SiO_2$ catalysts, J. Electron Spectrosc., 1979, 16, 267–276.
[41] McIntyre N. S., and Cook M. G., X-ray photoelectron studies on some oxides and hydroxides of cobalt, nickel, and copper, Anal. Chem., 1975, 47, 2208–2213.
[42] Occelli M. L., Psaras D., Suib S. L., and Stencel J. M., Metal contaminant effects on the properties of a silica-rich fluid cracking catalyst, Appl. Catal., 1986, 28, 143–160.

[43] Shalvoy R. B. and Reucroft P. J., Characterization of coprecipitated nickel on silica methanation catalysts by X-ray photoelectron spectroscopy, J. Catal., 1979, 56, 336–348.

[44] Hadjiivanov K. I. and Vayssilov G. N., Characterization of oxide surfaces and zeolites by carbon monoxide as an IR probe molecule, Adv. Catal., 2002, 47, 308–511.

[45] Kuznetsova T. G., Sadykov V. A., Moroz E. M., Trukhan S.N., Paukshtis E.A., Kolomiichuk V.N., et al., Preparation of Ce-Zr-O composites by a polymerized complex method, Stud. Surf. Sci. Catal., 2000, 143, 659–667.

[46] Hadjiivanov K., Mihaylov M., Abadjieva N., and Klissurski D., Characterization of Ni/TiO_2 catalysts prepared by successive adsorption–reduction of Ni^{2+} ions, J. Chem. Soc., Faraday Trans., 1998, 94, 3711–3716.

[47] Kasai P. H., Bishop R. J., and McLeod D., Ligand effects on the redox reactions in nickel- and copper-exchanged zeolites, J. Phys. Chem., 1978, 82, 279–285.

[48] Escalona Platero E., Colluccia S., and Zecchina A., Dipole coupling and chemical shifts in CO overlayers adsorbed on NiO, Surf. Sci., 1986, 171, 465-482.

[49] Jensen M. B., Morandi S., Prinetto F., Olafsen Sjastad A., Olsbye U., and Ghiotti G., FT-IR characterization of supported Ni-catalysts: influence of different supports on the metal phase properties, Catal. Today, 2012, 197, 38–49.

[50] Peri J. B., Infrared studies of Ni held at low concentrations on alumina supports, J. Catal., 1984, 86, 84–94.

[51] Paukshtis E. A., Yurchenko E. N., Study of the acid–base properties of heterogeneous catalysts by infrared spectroscopy, Russ. Chem. Rev., 1983, 52, 242–258

[52] Montini T., Bañares M.A., Hickey N., Di Monte R., Fornasiero P., Kašpar J., et al., Promotion of reduction in $Ce_{0.5}Zr_{0.5}O_2$: the pyrochlore structure as effect rather than cause? Phys. Chem. Chem. Phys., 2004, 6, 1-3.

[53] Richardson J. T., Twigg M.V., Reduction of impregnated NiO/ ⟨-Al_2O_3. Association of Al^{3+} ions with NiO, Appl. Catal. A-Gen., 1998, 167, 57-64.

[54] Bobrova L.N., Bobin A.S., Mezentseva N.V., Sadykov V.A., Thybaut J.W., Marin G.B., Kinetic assessment of dry reforming of methane on Pt + Ni containing composite of fluorite-like structure, Appl. Catal. B-Environ., 2016, 182, 513–524.

[55] Sadykov V., Rogov V., Ermakova E., Arendarsky D., Mezentseva N., Alikina G., et al., Mechanism of CH_4 Dry Reforming by Pulse Microcalorimetry: metal nanoparticles on perovskite/fluorite supports with high oxygen mobility, Thermochim. Acta, 2013, 567, 27– 34.

[56] Bobin A. S., Sadykov V. A., Rogov V. A., Mezentseva N. V., Alikina G. M., Sadovskaya E. M., et al., Mechanism of CH_4 dry reforming on nanocrystalline doped ceria-zirconia with supported Pt, Ru, Ni, and Ni–Ru, Top. Catal., 2013, 56, 958–968.